

Advanced Modulation Techniques for Flexible Optical Transceivers: The Rate/Reach Tradeoff

*Original*

Advanced Modulation Techniques for Flexible Optical Transceivers: The Rate/Reach Tradeoff / Bosco, G.. - In: JOURNAL OF LIGHTWAVE TECHNOLOGY. - ISSN 0733-8724. - STAMPA. - 37:1(2019), pp. 36-49.  
[10.1109/JLT.2018.2886257]

*Availability:*

This version is available at: 11583/2742116 since: 2019-07-16T13:12:06Z

*Publisher:*

Institute of Electrical and Electronics Engineers Inc.

*Published*

DOI:10.1109/JLT.2018.2886257

*Terms of use:*

This article is made available under terms and conditions as specified in the corresponding bibliographic description in the repository

*Publisher copyright*

IEEE postprint/Author's Accepted Manuscript

©2019 IEEE. Personal use of this material is permitted. Permission from IEEE must be obtained for all other uses, in any current or future media, including reprinting/republishing this material for advertising or promotional purposes, creating new collecting works, for resale or lists, or reuse of any copyrighted component of this work in other works.

(Article begins on next page)

# Advanced Modulation Techniques for Flexible Optical Transceivers: the Rate/Reach Trade-off

Gabriella Bosco, *Fellow, IEEE, Fellow, OSA*

(Invited Tutorial)

**Abstract**—This tutorial paper reviews advanced modulation techniques that have been proposed in the literature for the implementation of flexible (or reconfigurable) transceivers, which are fundamental building blocks of next-generation software-defined optical networks. Using a common reference multi-span propagation system scenario, the performance of transceivers employing standard quadrature-amplitude modulation with variable-rate forward error correction, probabilistic constellation shaping and time-domain hybrid formats is assessed, highlighting the achievable flexibility in terms of continuous trade-off between transmission rate and distance. The combination of these techniques with sub-carrier multiplexing, which enables an increase of the fiber nonlinearity tolerance thanks to the optimization of the symbol rate per sub-carrier, is also discussed.

**Index Terms**—Optical fiber communication, modulation formats, coherent detection, flexible optical transceivers, probabilistic shaping, hybrid QAM, subcarrier multiplexing.

## I. INTRODUCTION

**T**HANKS to the deployment of optical transceivers based on the use of high-order modulation formats with coherent detection and advanced digital signal processing (DSP) techniques, the capacity of optical networks experienced a huge growth in the past few years [1]. A significant increase in transmission reach was achieved, thanks to the efficient compensation of linear and nonlinear system impairments in the digital domain [2]. In addition, optical systems employing coherent transceivers are characterized by a high level of flexibility with respect to legacy direct-detection systems, for the following reasons: (i) no optical dispersion management is needed, since the optimum performance is achieved in uncompensated systems; (ii) adaptive high-order modulation formats with fine granularity can be generated and detected; (iii) the same hardware can be used for different modulation formats.

In parallel, since the huge amount of traffic foreseen for the near future cannot be efficiently supported by static increases in network capacity, optical transport networks are currently migrating from a static configuration with little flexibility to the concept of software-defined optical networks [3]. In this scenario, a key role will be played by flexible and scalable coherent transceivers, able to dynamically adapt the modulation format and the transmission rate to the network conditions [4]–[11].

Today's coherent optical transceivers typically use a set of different modulation formats based on standard quadrature

amplitude modulation (QAM), generated through the combination of two pulse-amplitude modulation (PAM) formats in the in-phase and quadrature components. For these standard QAM formats, a gap to Shannon capacity exists, which can be expressed in terms of a penalty in signal-to-noise ratio (SNR). In addition, the standard QAM formats only offer a coarse granularity in spectral efficiency and, consequently, a coarse granularity in the achievable transmission reach. To overcome the lack in granularity, several techniques are currently under study, which take advantage of the high flexibility provided by commercially available high-speed digital-to-analog converters (DACs), allowing to fully design the transmitted signal in the digital/electrical domain. This means that, using the same hardware, different modulation formats can be generated and different transmission rates can be achieved. Examples of techniques used to increase the flexibility of optical transceivers are: variable code-rate transceivers [12]–[16], probabilistic constellation shaping (PS) [17]–[23] and time-domain hybrid formats (TDHF) [24]–[31]. The use of subcarrier multiplexing (SCM) [32]–[37], i.e. the decomposition of a single channel into several digital subcarriers, has also been proposed, as a means to increase the tolerance to nonlinear propagation effects, exploiting the symbol rate optimization (SRO) phenomenon [38]. A great advantage of all these methods is that the flexibility is achieved without requiring any additional hardware, thus allowing to reuse currently available single-carrier transceivers by simply reprogramming the transmitted signal in the digital domain.

The key design parameters to optimally exploit all available resources in long-haul and high-capacity optical transmission systems with coherent detection are the transmission rate, which is directly proportional to the spectral efficiency (SE) [39], and the maximum transmission reach. Multi-level modulation with coherent detection maximizes SE and transmission rate, improving the tolerance to transmission impairments by enabling effective, low-complexity electrical compensation of these impairments [40]. In wavelength-division multiplexing (WDM) optical systems, SE and total transmission rate can be increased by minimizing the frequency spacing between WDM channels (e.g. using the Nyquist-WDM technique [41], [42]), increasing the modulation cardinality or using forward error correction (FEC) codes with low overhead. In turn, the maximum transmission reach can be increased by using energy-efficient modulation formats (e.g. low-cardinality QAM) which reduce the SNR requirements at the receiver, using FEC codes with high overhead to ensure reliable transmission or applying proper techniques to mitigate the nonlinear propagation effects in the optical fiber.

In practice, a compromise has to be made between net transmission rate and achievable reach. For example, a transceiver that operates on a short network segment with high SNR can achieve a high SE to maximize the net data rate. Similarly, a transceiver operating on a long network segment with low SNR should use either a lower order modulation format or a FEC code with high overhead to ensure reliable transmission, at the expenses of a loss in SE and net data rate.

The rest of this paper is organized as follows. Section II gives an overview of the DSP-based coherent transceiver architecture. The system scenario and the performance metrics are described in Section III, while in Section IV three modulation schemes for flexible transceivers (QAM with variable code rate, PS and TDHF) are described and their performance assessed in a common multi-span link configuration. The three modulation formats are then compared in Section V in terms of rate/reach trade-off and flexibility. Section VI discusses the use of sub-carrier multiplexing and concluding remarks are given in Section VII.

## II. COHERENT TRANSCEIVERS ARCHITECTURE

The general structure of a dual-polarization coherent transceiver that can be used to generate high-order complex modulation formats is shown in Fig. 1. The four arrows/paths are referred to the in-phase and quadrature components of the two orthogonal polarizations of the transmitted modulation format. The transmitter (Tx) consists of a laser, a 4-channel high-speed digital-to-analog converter (DAC) [43] which generates the electrical driving signals defined by the Tx DSP unit, and a dual-polarization in-phase and quadrature (IQ) modulator [44]. The receiver (Rx) is composed of a local oscillator (LO) laser, an optical coherent front-end (including a polarization-diversity 90-degree hybrid and four balanced photo-detectors [45]) and a 4-channel high-speed analog-to-digital converter (ADC) [43], which generates the signals that are processed by the Rx DSP unit [2]. Using this hardware configuration, different modulation formats can be generated and, consequently, different transmission rates can be achieved. The flexibility is provided by changing the DSP algorithms, both at the Tx and at the Rx side. In the following, the transceiver blocks are briefly described, highlighting the critical points that have to be considered if the same hardware components are used to generate and detect modulation formats with different cardinality.

### *Tx laser and LO*

Phase noise induced by a non zero linewidth  $\Delta\nu$  of a laser is a major impairment in coherent optical communications, where both the phase and amplitude of the optical field are modulated. The impact of phase noise on system performance increases with the modulation format order [46], [47] and decreases with the symbol rate  $R_s$  (the higher the product between  $\Delta\nu$  and the symbol time  $T_s = 1/R_s$ , the higher the penalty due to phase noise). Note that, in a multi-format transceiver, the Tx laser and LO characteristics should be compliant with the requirements of the highest-order modulation format.

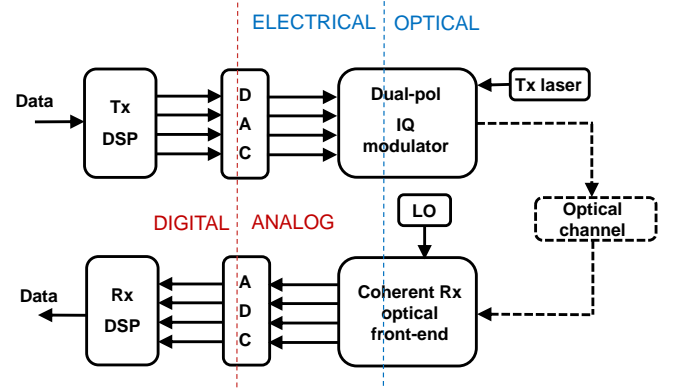


Fig. 1. GMI vs. SNR for 16QAM modulation. The five dots indicate the operating points corresponding to the five FEC schemes described in Table I.

### *Tx DSP*

One of the main functions of the DSP at the Tx side is to perform spectral shaping on the transmitted pulses [42], [48], [49], in order to increase the SE by reducing the spacing between the WDM channels. In addition, several system impairments can be pre-compensated by the Tx DSP, including bandwidth limitations [50], [51], transmitter IQ-skew [51], [52], non-linear transfer function of the Mach-Zehnder modulator [53], [54], chromatic dispersion (CD) [55], [56] and non-linear propagation effects [57]–[59]. All these algorithms are modulation-format independent, thus the same DSP can be applied to all formats.

### *Rx DSP*

The Rx DSP operations may vary, depending on the particular realization of the receiver, however the generic DSP procedures are similar and can be summarized as [60]–[62] :

- IQ imbalances correction: compensation of the mismatch of amplitude, phase and timing between in-phase and quadrature components.
- CD compensation and static channel equalization: compensation of bulk chromatic dispersion and static filtering effects.
- Dynamic channel equalization: polarization demultiplexing and compensation of polarization mode dispersion (PMD), residual CD and bandwidth limitations.
- Timing recovery: estimation and correction of the timing errors.
- Frequency offset estimation (FOE): estimation and compensation of the frequency mismatch between Tx laser and LO.
- Carrier phase estimation (CPE): estimation and compensation of the laser phase noise.
- Decoding, decision and demapping: FEC decoding and estimation of transmitted bits.

In flexible transceivers, the DSP algorithms have to support different modulation formats. In this regard, the above mentioned functions can be roughly divided into two groups: (i) DSP functions that can be realized by algorithms that naturally

work format-independent since they do not depend on the constellation (e.g. IQ imbalance correction, CD estimation and compensation, timing and carrier frequency recovery); (ii) DSP functions that are naturally format-dependent since they are operating on the constellation (e.g. symbol decision, dynamic equalizer and CPE).

The design of the adaptive equalizer and the CPE algorithm is particularly challenging [63], since popular blind time-domain equalizers use filter update strategies matched to the specific modulation format [64], [65] and CPE algorithms that are suitable for arbitrary PM-QAM formats and most 4D modulation formats may become too complex when a large size of the constellation is considered [46], [66]. It has been shown that the use of data-aided algorithms may be a reasonable way to a cost-efficient and format-independent implementation of dynamic equalizer and CPE in flexible transceivers [63]. These algorithms are typically based on the use of either known or pilot symbols [67]–[69] or pilot tones [70], [71] that are inserted in the payload at the transmitter at the cost of an additional overhead. At the receiver, the pilot information is evaluated independently of the payload and its modulation format.

#### DAC and ADC

High speed DACs and ADCs are key elements in DSP-based coherent optical transceivers. They are both characterized by a sampling frequency  $f_s$ , an analog bandwidth  $B$ , and a physical bit resolution  $n_{bit}$ . The number of bits per symbol  $n_{bps}$  of the digitized version of a modulated signal with symbol rate  $R_s$  is equal to the ratio between the DAC or ADC sampling frequency and  $R_s$ :  $n_{bps} = f_s/R_s$ . In order to generate and detect multi-level modulation formats, DACs and ADCs with a high number of resolution bits are required [46], with the necessary resolution increasing approximately by 1 bit when the number of constellation points is multiplied by 4 [40]. Typically, DSP algorithms work with  $n_{bps} = 2$  samp/symb, but operation with lower values has been demonstrated [72], [73], enabled by the use of anti-aliasing electrical filters specifically designed to limit the penalty due to spectrum replica. Note that the required bandwidth of these filters varies with the symbol rate.

#### *IQ modulator*

The most common configuration of the IQ modulator employs two parallel Mach-Zehnder modulators (MZM) that are driven by the electrical signals corresponding to the in-phase and quadrature component of the information signal, respectively. An optical phase shift of  $\pi/2$  is applied to the lower branch before recombining the two outputs [74]. In order to generate a polarization-multiplexed (PM) signal, two parallel IQ modulators are used, with a single laser output split by a polarization beam splitter (PBS). The two outputs of the IQ modulators are then combined by a polarization beam combiner (PBC) and transmitted through the fiber.

Note that, in order to generate multi-level modulation formats, the linearity of the modulator is a fundamental requirement. Since the transfer function of the MZM is intrinsically

non-linear, two options are available: (i) Operate the modulator in the linear regime, reducing the driving voltage range (with the undesired consequence of decreasing the OSNR at the output of the modulator). (ii) Operate the modulator in the nonlinear region, applying a pre-distortion to the modulating signal in the digital domain [53], [54].

Another key parameter of a MZM is the extinction ratio (ER), defined as the ratio between the maximum and minimum optical intensities measured at the modulator output. Poor ERs will induce chirp (an optical phase variation due to relative variation of optical intensity) in the optical signal. The presence of chirp in a transmitted signal will distort the transitions between constellation points and increase the minimum required OSNR for the system. With closely spaced constellation points, higher order modulation formats will require better ERs than lower cardinality formats.

#### *Coherent Rx optical front-end*

The optical front-end is used to linearly map the incoming optical signal into four electrical signals, corresponding to the in-phase and quadrature field components for the two polarizations. It employs two polarization beam splitters and a pair of 90-degree hybrids, one for each component of polarization [44]. The light of the received information signal is combined with a LO [2], generating eight output signals (four for each optical hybrid) that are then detected by four balanced photodiodes.

Since the analog electronic and opto-electronic parts of a transceiver are usually designed for a specific target symbol rate, it is reasonable to assume that a cost-efficient realization of a flexible transceiver operates at a fixed symbol rate. The analyses reported in the following sections assume a fixed symbol rate (64 Gbaud) for all considered modulation schemes.

### III. PERFORMANCE METRICS

In Section IV, the performance of different modulation techniques will be assessed and compared, in terms of flexibility and rate/reach trade-off. We report in the following the definition of the metrics that are used to evaluate the system performance, which are based on the following assumptions:

- Soft-decision binary FEC codes are used.
- The residual channel memory after the receiver digital filters is negligible.
- The optical channel is represented towards the FEC as a memory-less additive white Gaussian noise (AWGN) channel.

#### *A. Back-to-Back Performance*

When using soft-decision binary FEC codes, the generalized mutual information (GMI), together with its normalized version NGMI [14], [75], are reliable parameters for the estimation of the post-FEC performance of the systems, without the need of implementing the encoder/decoder pair. In our analyses, the back-to-back performance is assessed in terms

TABLE I  
OVERALL RATE AND NORMALIZED GMI REQUIRED FOR LDPC CODES WITH DIFFERENT CODE RATES  $r_{FEC}$  THAT ARE CONCATENATED WITH A STAIRCASE CODE TO ACHIEVE A BER OF  $10^{-15}$  AFTER DECODING [76].

Code #	LDPC code rate $r_{LDPC}$	Threshold NGMI $NGMI_{th}$	Overall rate $r_{FEC}$
1	0.71	0.75	0.67
2	0.75	0.78	0.71
3	0.81	0.84	0.76
4	0.86	0.88	0.81
5	0.90	0.92	0.85

of the GMI, estimated through Monte-Carlo simulation, as a function of the signal-to-noise ratio (SNR), defined as:

$$SNR = \frac{P_{ch}}{2N_0R_s} \quad (1)$$

where  $P_{ch}$  is the power of the polarization-multiplexed signal at the input of the receiver,  $N_0$  is the one-sided power spectral density (PSD) of noise and  $R_s$  is the symbol rate. The GMI, measured in bits/symb, represents the maximum number of information bits per transmitted symbol. Once the GMI has been estimated, the normalized generalized mutual information (NGMI), which represents the maximum number of information bits per transmitted bit, can be derived. Note that the relationship between GMI and NGMI can be different for uniform and PS constellations, as shown in the following.

1) *Uniform QAM*: The NGMI is obtained dividing the GMI by the number of bits per symbol  $m$ :

$$NGMI = \frac{GMI}{m} \quad (2)$$

In practice, an ideal (infinite-length) binary FEC code with rate  $r_{FEC}$  permits error-free decoding if the channel quality satisfies  $NGMI > r_{FEC}$ . For an ideal binary FEC code, the code rate  $r_{FEC}$  can thus be interpreted as its NGMI threshold. For realistic FEC implementations, the NGMI threshold is typically higher than the code rate, as shown in [76] where several realistic FEC code schemes are described, based on a concatenation of an inner LDPC code and an outer staircase code with fixed 6.25% overhead [77]. Table I reports, for different rates of the inner LDPC code, the value of the threshold NGMI, as well as the overall rate of the concatenation of the two codes.

When using a given FEC scheme, with code rate  $r_{FEC}$  and NGMI threshold  $NGMI_{th}$ , a single operating point can be identified on each GMI vs. SNR curve, corresponding to  $GMI = m \cdot NGMI_{th}$ . As an example, Fig. 2 shows the GMI vs. SNR curve for a 16QAM modulation format. The dots show the five operating points corresponding to the five FEC schemes of Table I. Each of the operating points in Fig. 2 corresponds to a net transmission rate  $R_{QAM}$  (in Gbit/s) of the QAM signal, which can be obtained as:

$$R_{QAM} = m \cdot r_{FEC} \cdot R_s \quad (3)$$

2) *Probabilistically-Shaped QAM*: The relationship between GMI and NGMI shown in Eq. (2), as well as the relationship between the net data rate and the FEC rate shown in Eq. (3), are valid for uniformly distributed modulation

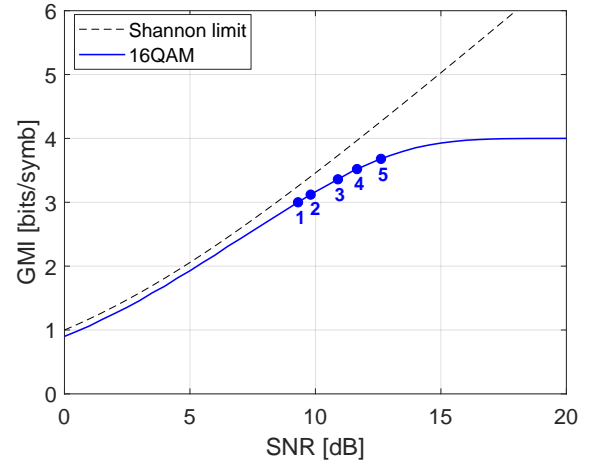


Fig. 2. Ideal back-to-back performance of 16QAM modulation. The five dots indicate the operating points corresponding to the five FEC schemes described in Table I.

formats only. When using PS symbols, generated with the probabilistic amplitude shaping (PAS) algorithm described in [78], the net data rate is related to the FEC rate through the following equation (see [18], Eq. (25)):

$$R_{PS-QAM} = [H(P) - (1 - r_{FEC}) \cdot m] \cdot R_s \quad (4)$$

where  $H(P)$  is the entropy of the probabilistically shaped constellation. Substituting  $R_{PS-QAM}/R_s$  with GMI and  $r_{FEC}$  with NGMI [75], the following relationship between GMI and NGMI is obtained:

$$\begin{aligned} GMI &= H(P) - (1 - NGMI) \cdot m = \\ &= NGMI \cdot m - [m - H(P)] \end{aligned} \quad (5)$$

Inverting the previous equation:

$$NGMI = \frac{GMI}{m} + \left[1 - \frac{H(P)}{m}\right] \quad (6)$$

### B. Multi-Span Propagation Performance

The performance after non-linear propagation over an optically amplified multi-span system was estimated using the EGN model [79], [80], with the following assumptions on the system setup (which are summarized in Table II and are the same for all studied modulation schemes):

- Symbol rate of a single channel of the WDM comb:  $R_s=64$  Gbaud.
- Spectral shape: root raised-cosine (RRC) with roll-off 0.15.
- Frequency spacing between the WDM channels:  $\Delta f=75$  GHz.
- WDM transmission over the entire C-band (total bandwidth equal to  $\sim 4.5$  THz).
- Fiber type: standard single-mode fiber (SSMF), with attenuation  $\alpha=0.2$  dB/km, dispersion  $D=16.7$  ps/nm/km, non-linearity coefficient  $\gamma=1.3$  1/W/km.
- Fiber span: 100 km, with total attenuation of 21 dB, which includes losses due to splices and connectors.

TABLE II  
SYSTEM PARAMETERS.

Parameter	Value
Symbol rate	64 Gbaud
Polarization	Dual polarization
Pulse shape	Root raised-cosine (RRC)
RRC roll-off	0.15
Number of WDM channels	60 (EGN model) 20 (simulations)
WDM spacing	75 GHz
Nonlinear coefficient $\gamma$	1.3 1/W/km
Dispersion $D$	16.7 ps/nm/km
Fiber loss $\alpha$	0.2 dB/km
Total span loss	21 dB
Span length $L_s$	100 km
Amplification	EDFA
EDFA noise figure	5 dB
Laser linewidth	10 kHz

- EDFA lumped amplification (noise figure  $F = 5$  dB), whose gain  $G$  completely recovers the span loss.
- Tx laser and LO linewidth: 10 kHz.
- 2-dB SNR penalty with respect to the ideal performance, which takes into account the impairments of a realistic transceiver.

According to the EGN model, the SNR after non-linear propagation, which includes both the linear and non-linear noise terms, is given by [81]:

$$\text{SNR}_{\text{NL}} = \frac{P_{ch}}{P_{\text{ASE}} + P_{\text{NLI}}} \quad (7)$$

where  $P_{\text{ASE}}$  is the power of the ASE noise introduced by the optical amplifiers:

$$P_{\text{ASE}} = Fh\nu(G - 1)R_sN_s \quad (8)$$

where  $h$  is the Planck's constant and  $\nu$  is the center propagation frequency.  $P_{\text{NLI}}$  is the power of the non-linear interference (NLI):

$$P_{\text{NLI}} = \int G_{\text{NLI}}(f)df \quad (9)$$

where  $G_{\text{NLI}}(f)$  is the PSD of the NLI noise (which is a function of the number of spans  $N_s$ ). The results shown in this paper have been obtained using Eqs. (1) and (2) in [82] for the evaluation of the NLI term, i.e., subtracting the following *format-dependent* term from the *format-independent*  $P_{\text{NLI}}$  estimated using the GN-model [83]:

$$P_{\text{corr}} = \frac{80}{81} \Phi \frac{\gamma^2 L_{\text{eff}}^2 P_{ch}^2 N_s}{R_s \Delta f \pi \beta_2 L_s} \text{HN} \left( \frac{N_{ch} - 1}{2} \right) \quad (10)$$

where  $L_{\text{eff}}$  is the effective length of the fiber,  $\beta_2$  is the dispersion coefficient in [ps<sup>2</sup>/km],  $N_{ch}$  is the number of WDM channels and HN is the harmonic number series, defined as  $\text{HN} = \sum_{n=1}^N (1/n)$ .  $\Phi$  is a factor that depends on the fourth standardized moment  $\hat{\mu}_4$  of the transmitted symbols  $X$ :

$$\Phi = 2 - \hat{\mu}_4 = 2 - \frac{E[|X - E[X]|^4]}{(E[|X - E[X]|^2])^2} \quad (11)$$

$\Phi$  is equal to 1 for phase-shift-keying (PSK) formats, such as quadrature phase-shift-keying (QPSK), and goes down to

TABLE III  
VALUES OF ENTROPY  $H(P)$  AND PARAMETER  $\Phi$  IN EQ. (10) FOR QAM MODULATIONS.

QAM format	H(P) [bits/symb]	$\Phi$
QPSK	2	1.000
8QAM	3	0.666
16QAM	4	0.680
32QAM	5	0.690
64QAM	6	0.619
128QAM	7	0.657
256QAM	8	0.605

zero for an ideal Gaussian constellation. For QAM modulation formats, it decreases with the constellation cardinality, approaching 0.6 for an infinite number of points. The values of  $\Phi$  for all modulation formats considered in this paper can be found in Tables III, V and VI.

Monte-Carlo numerical simulations were also performed in a few selected cases, using the time-domain split-step Fourier method for fiber propagation. A decision-directed least-mean square (LMS) dynamic equalizer with 30 taps was used, followed by carrier phase estimation based on the BPS algorithm, with an averaging window of 100 symbols. In the simulations, the same system parameters detailed above were used. The only difference was the number of WDM channels that, due to simulation time constraints, was decreased from 60 to 20, corresponding to a total WDM bandwidth of approximately 1.5 THz.

#### IV. MODULATION SCHEMES FOR FLEXIBLE TRANSCEIVERS

Using PM-M-QAM formats with variable cardinality  $M$  at a fixed symbol rate and with a fixed-rate code scheme, the achievable net data rate can change only in coarse discrete steps. As an example, at 64 Gbaud and using an FEC code with 28% FEC overhead, a net data rate of 200 Gbit/s can be achieved with PM-QPSK, 300 Gbit/s with PM-8QAM, 400 Gbit/s with PM-16QAM, 500 Gbit/s with PM-32QAM, 600 Gbit/s with PM-64QAM, 700 Gbit/s with PM-128QAM and 800 Gbit/s with PM-256QAM. In practice, the output data rate can be changed only in steps of 100 Gbit/s (i.e.  $2R_s r_{\text{FEC}}$ ), due to the discrete variation in number of bits per symbol of standard QAM modulation formats. In order to achieve a continuous trade-off between spectral efficiency and distance, keeping the symbol rate fixed, two options are available: (i) use variable-rate forward error correction (FEC) code, as proposed in [12]; (ii) use advanced modulation techniques that allow to achieve fractional numbers of bits per symbol. In subsection IV-A, the first option is investigated, considering combinations of standard QAM formats and the five FEC schemes described in Table I (similar analyses can also be found in [12]–[16]). The second option is investigated in Sections IV-B and IV-C, where the performance of optical systems based on the use of either PS or TDHF is assessed. The system scenario, described in Section III, is the same in all cases.

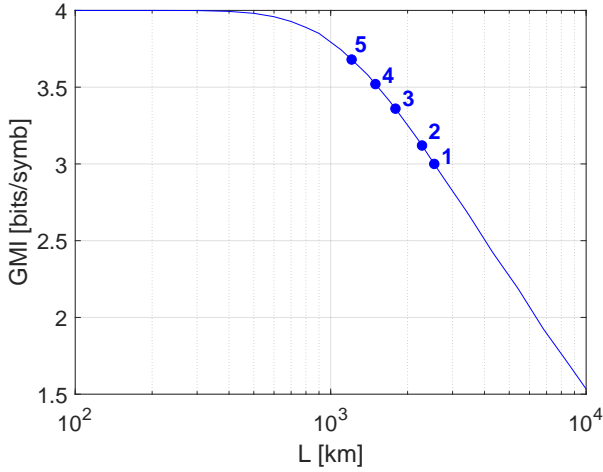


Fig. 3. GMI as a function of the length of the fiber link for 16QAM modulation. The system parameters are reported in Table II. The five dots indicate the operating points corresponding to the five FEC schemes described in Table I.

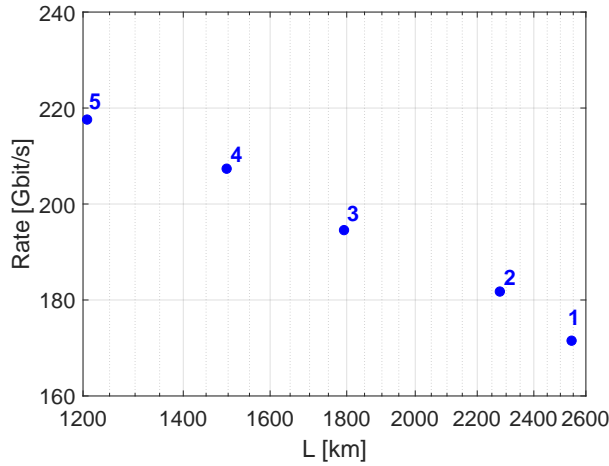


Fig. 4. Net data rate as a function of the length of the fiber link for 16QAM modulation. Each point corresponds to one of the five FEC schemes described in Table I.

#### A. Standard PM-QAM Formats with Variable Code-Rate

Fig. 3 shows the long-haul propagation performance of the PM-16QAM modulation, in terms of GMI as a function of the multi-span fiber link length. The system parameters are reported in Table II. The GMI vs.  $L$  curve was generated by estimating the values of the SNR (see Eq. (7)) after each span using the EGN model and then obtaining the corresponding GMI values through the back-to-back curve (see Fig. 2). The five dots indicate the operating points corresponding to the five FEC schemes described in Table I. Each of these points corresponds to a net data rate, that can be obtained using Eq. (3). The available combinations of rate and distance are shown in Fig. 4, where the trade-off between rate and distance is clearly shown.

Similar operations can be performed for all QAM modulation formats, in order to increase the range of available rates and distances. Table IV reports all combinations of modulation formats and code rates that have been used in order to span the

TABLE IV  
NET DATA RATE, MAXIMUM NUMBER OF SPANS AND CORRESPONDING VALUE OF SNR FOR SEVERAL COMBINATIONS OF PM-QAM MODULATION FORMATS AND FEC SCHEMES.

Format	Code	Rate [Gbit/s]	$N_s$	SNR [dB]
QPSK	1	171.5	101	5.4
QPSK	2	181.8	92	5.8
QPSK	3	194.6	76	6.7
QPSK	4	207.4	65	7.4
QPSK	5	217.6	54	8.2
8QAM	1	257.3	41	9.1
8QAM	2	272.6	37	9.6
8QAM	3	291.8	29	10.7
16QAM	1	343.0	25	11.3
16QAM	2	363.5	22	11.8
16QAM	3	389.1	17	12.9
16QAM	4	414.7	14	13.7
32QAM	2	454.4	11	14.7
32QAM	3	486.4	9	15.8
32QAM	4	518.4	7	16.6
64QAM	2	545.3	6	17.0
64QAM	3	583.7	5	18.3
64QAM	4	622.1	4	19.2
64QAM	5	652.8	3	20.3
256QAM	2	727.0	2	22.0
256QAM	4	829.4	1	24.6

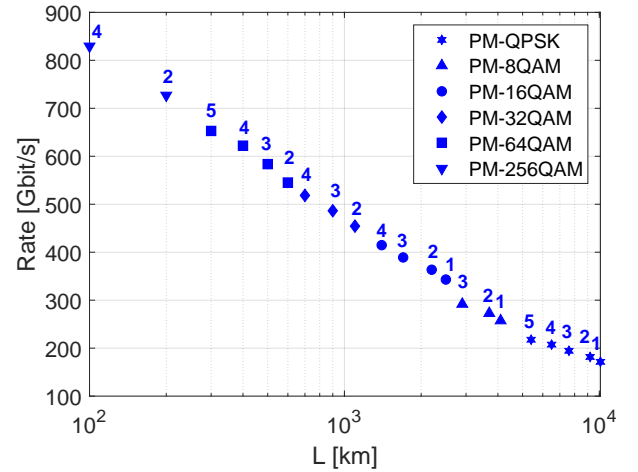


Fig. 5. Net data rate as a function of the transmission distance for the combinations of modulation formats and FEC codes shown in Table IV (the code number appears above each point). The number of WDM channels is 60, corresponding to a total bandwidth of  $\sim 4.5$  GHz.

system length from  $N_s=1$  to  $N_s=100$ . Note that not all possible combinations of modulation formats and FEC codes have been used, since some of them yielded very similar rate and/or transmission distance. In those cases, the lower cardinality modulation format and the higher code rate were selected, since they yield a lower complexity. The rate vs. reach results are summarized both in Fig. 5 and in Table IV, where, for each distance, the corresponding value of SNR is also shown.

In order to assess the impact of propagation effects on a realistic receiver DSP, a set of numerical simulations were run and the results shown in Fig. 6 for PM-QAM constellations with cardinality 16, 64 and 256. The blue solid lines show the predictions of the EGN model. The system and simulation parameters are described in Section III-B. The red cir-



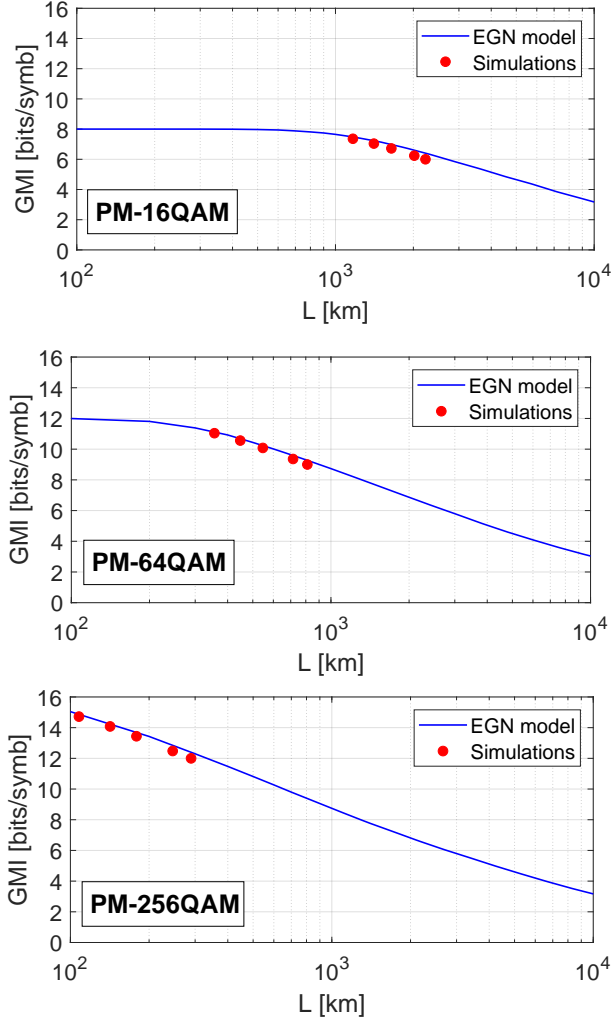


Fig. 6. Comparison between EGN model predictions (solid lines) and numerical simulation results (red circles), in terms of GMI vs. reach for PM-16QAM (top), PM-64QAM (middle) and PM-256QAM (bottom). The five dots correspond to the operating points related to the five FEC schemes described in Table I. The number of WDM channels is 20, corresponding to a total bandwidth of  $\sim 1.5$  GHz.

cles show the GMI values vs. transmission reach estimated through numerical simulations in the five operating points corresponding to FEC schemes in Table I. The accuracy of the EGN model predictions is in general good, with some penalty appearing for high code rates, due to the lower value of OSNR, and thus higher values of additive noise that hinder the performance of the adaptive DSP blocks (dynamic equalizer and CPE) and thus impair the achievable performance.

### B. Probabilistic Shaping (PS)

A PS-QAM constellations can be efficiently generated using the PAS scheme described in [78], which enables a separation of the design of FEC codes and PS, offering a near-optimal shaping gain when fixed-length data frame are used [84]. Using this scheme, QAM modulation symbols are generated and transmitted with different probabilities. The distribution that maximizes the SNR performance in a linear AWGN channel is the Maxwell-Bolzman distribution, according to which the

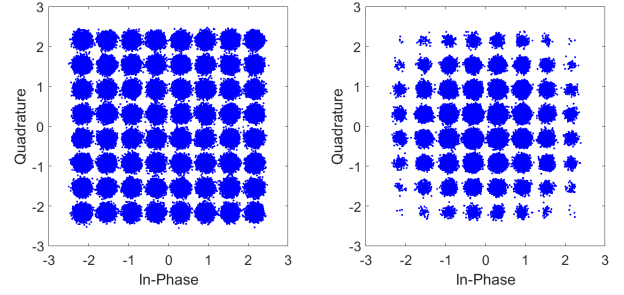


Fig. 7. Noisy scattering diagrams of uniformly distributed 64QAM (left) and PS-64QAM with  $H(P)=4.5$  bits/symb (right).

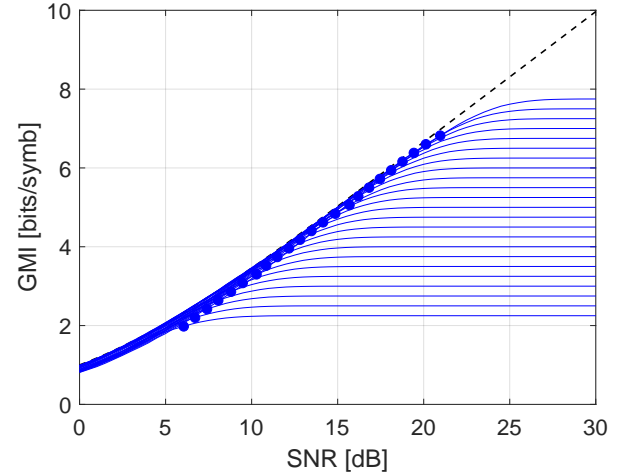


Fig. 8. Ideal back-to-back performance of PS formats, with values of  $H(P)$  ranging from 2.25 to 7.75 bits/symb with step 0.25 bits/symb. The dots indicate the operating points corresponding to the FEC code #4 in Table I.

probability of transmitting a symbol  $x \in \chi$  exponentially decreases with the energy of the symbol:

$$P(x) = ke^{-\lambda|x|^2} \quad (12)$$

An increase of the parameter  $\lambda$  increases the amount of shaping applied to the constellation, reducing its entropy:

$$H(P) = - \sum_{x \in \chi} P(x) \log_2 P(x) \quad (13)$$

and increasing its efficiency in a specific SNR region [23]. An example of PS constellation is shown in Fig. 7, where the noisy scattering diagram of a PS-64QAM with entropy equal to 4.5 bits/symb is compared to the uniformly distributed 64QAM constellation.

In this section, we analyze the performance of different PS schemes, generated from square QAM constellations with cardinality 16, 64 and 256. The parameter  $\lambda$  in Eq. (12) is tuned in order to obtain the desired constellation entropy. Fig. 8 shows the back-to-back performance of several PS formats, with values of  $H(P)$  ranging from 2.25 to 7.75 bits/symb with step 0.25 bits/symb. Each curve corresponds to a different format and it converges to the value of entropy for high SNRs. The dots indicate the operating points corresponding to the FEC code #4 in Table I. The GMI and, consequently,



TABLE V

VALUES OF ENTROPY  $H(P)$  AND PARAMETER  $\Phi$  IN EQ. (10) FOR PS MODULATIONS. THE ACHIEVABLE NET DATA RATE OF PM SIGNALS, THE MAXIMUM NUMBER OF SPANS THAT CAN BE REACHED AND THE CORRESPONDING SNR ARE ALSO SHOWN, UNDER THE ASSUMPTION THAT THE CODE #4 IN TABLE I IS USED.

Modulation format	$H(P)$ [bits/symb]	$\Phi$	Rate [Gbit/s]	$N_s$	SNR [dB]
PS-16QAM	2.25	0.585	190.7	75	8.1
PS-16QAM	2.5	0.281	222.7	58	8.7
PS-16QAM	2.75	0.139	254.7	46	9.4
PS-16QAM	3	0.113	286.7	37	10.1
PS-16QAM	3.25	0.166	318.7	30	10.8
PS-16QAM	3.5	0.27	350.7	25	11.5
PS-16QAM	3.75	0.41	382.7	20	12.3
PS-64QAM	4.25	0.01	398.1	18	13.5
PS-64QAM	4.5	0.026	430.1	14	14.2
PS-64QAM	4.75	0.058	462.1	12	14.8
PS-64QAM	5	0.107	494.1	10	15.5
PS-64QAM	5.25	0.176	526.1	8	16.1
PS-64QAM	5.5	0.263	558.1	7	16.9
PS-64QAM	5.75	0.382	590.1	6	17.7
PS-256QAM	6.25	0.012	605.4	5	18.8
PS-256QAM	6.5	0.029	637.4	4	19.5
PS-256QAM	7	0.111	701.4	3	20.8
PS-256QAM	7.5	0.265	765.4	2	22.1
PS-256QAM	7.75	0.392	797.4	1	23.0

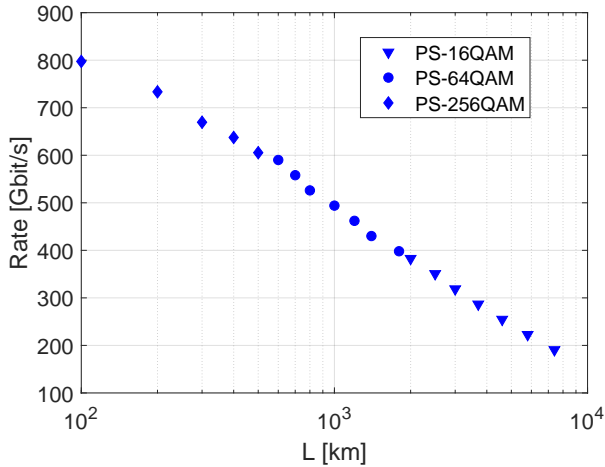


Fig. 9. Net data rate of polarization-multiplexed PS formats vs. distance when the FEC code #4 in Table I is used. The blue markers (from the right to the left) corresponds to the modulation formats reported in Table V (from the top to the bottom). The number of WDM channels is 60, corresponding to a total bandwidth of  $\sim 4.5$  GHz.

the transmit rate, can be dynamically “tuned” keeping the same FEC scheme and constellation (therefore, the same DSP algorithms).

The net data rate vs. distance curve is shown in Fig. 9 for all the formats described in Table V. The points (from the right to the left) corresponds to the modulation formats reported in the table (from the top to the bottom). Note that at 1 span (100 km), the PS format seems to have worse performance than the uniform QAM format (see Fig. 5). The reason for this apparently strange behavior is the quantization of the maximum reach values, which are integer multiples of the span length. Even though the performance of PS-256QAM is better than the one achievable with uniform 256QAM, it is not

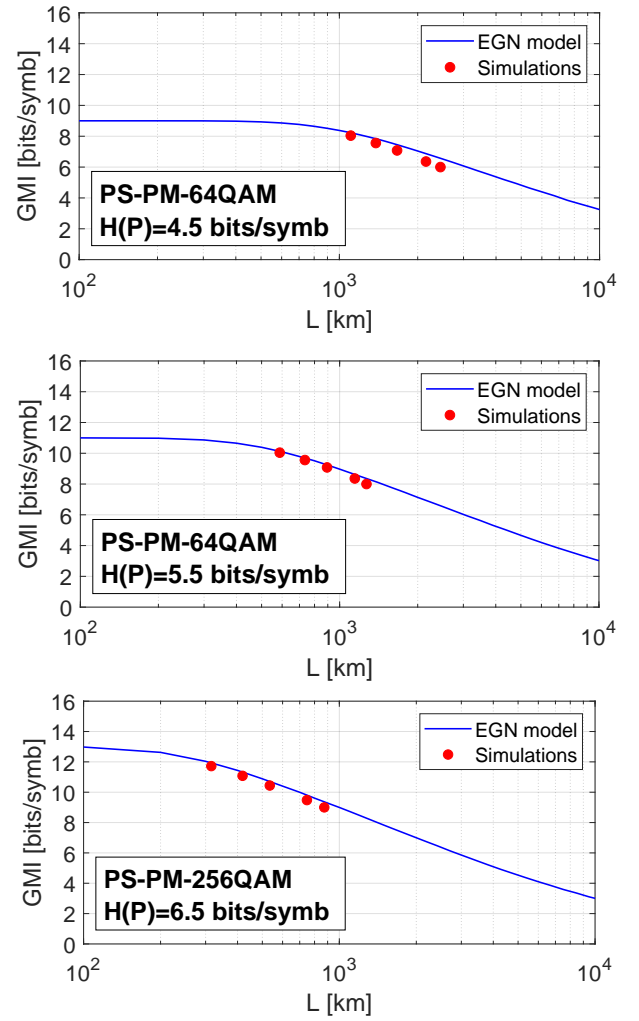


Fig. 10. Comparison between EGN model predictions (solid lines) and numerical simulation results (red circles), in terms of GMI vs. reach for three PS modulation formats. The five dots correspond to the operating points related to the five FEC schemes described in Table I. The number of WDM channels is 20, corresponding to a total bandwidth of  $\sim 1.5$  GHz.

sufficiently good to reach 2 spans at  $H(P)=7.75$  bit/symb, thus the performance in terms of maximum number of spans is the same as for PM-256QAM.

Similar to what done for uniformly distributed formats, a set of numerical simulations were run in order to assess the impact of propagation effects on a realistic receiver DSP. The results are shown in Fig. 10 for PS-QAM constellations with entropy equal to 4.5, 5.5 or 6.5 bits/symb. The blue solid lines show the predictions of the EGN model (the systems parameters are reported in Table II). The red circles show the GMI values vs. transmission reach estimated through numerical simulations in the five operating points corresponding to FEC schemes in Table I. The system parameters and Rx DSP (described in Section III) are the same as for standard QAM formats. Also in this case, some penalty with respect to the EGN model predictions appears for high code rates, due to the lower value of OSNR, and thus higher values of additive noise that hinder the performance of the adaptive DSP blocks (dynamic equalizer and CPE) and thus impair the achievable

performance. Since the ratio between the laser linewidth (10 kHz) and the symbol rate (64 Gbaud) is relatively small, the optimum length of CPE averaging window is quite large (around 100 symbols). This means that most of the nonlinear phase noise is not compensated for by the CPE algorithm. Being characterized by a lower value of the parameter  $\Phi$ , PS formats are in general more impacted by nonlinear phase noise than uniform QAM formats, as discussed in [20].

### C. Time-Domain Hybrid-Formats (TDHF)

The TDHF technique consists in transmitting different modulation formats with symbols interleaved in the time domain. By changing the ratio of symbols carrying the different modulation formats, the spectral efficiency can be adjusted in fine steps [27]. In this way, a high degree of flexibility is achieved, since the transmission rate and, consequently, the SNR performance can be tuned by simply modifying the pattern of the QAM formats.

The TDHF schemes considered in this paper transmit two different QAM formats interleaved in the time domain. Each periodic frame is considered to be composed of  $N$  symbols distributed among two neighboring square QAM modulation formats with constellation sizes  $M_1$  and  $M_2$ . The TDHF frame is characterized by a given format ratio,  $K = N_1/N_2$ , where  $N_1$  represents the number of symbols occupied by the modulation format with the lowest constellation size  $M_1$ . The entropy  $H$  of the dual-polarization TDHF constellation, which corresponds to the maximum number of bits per symbol that can be transmitted, can be fine tuned by varying the parameters  $M_1$ ,  $M_2$ ,  $N_1$  and  $N_2$ , as:

$$H = 2 \frac{\log_2(M_1)N_1 + \log_2(M_2)N_2}{N_1 + N_2} \quad (14)$$

A key parameter for TDHFs is the power ratio (PR) between the two employed modulation formats, defined as:

$$\text{PR} = \frac{P_2}{P_1}. \quad (15)$$

where  $P_1$  and  $P_2$  are the power of the lowest and highest cardinality QAM formats, respectively. The values of PR used in this work are the ones that maximize the back-to-back performance in terms of GMI vs. SNR in the region of operation corresponding to the FEC code #4 in Table I. The optimum power ratio value is typically close to the value that guarantees the same SNR performance for both QAM formats [29]. Since the higher order QAM is more sensitive to noise than the lower order QAM, PR always assume values higher than 1.

Table VI reports the parameters of the TDHF schemes that have been considered, together with the values of the parameter  $\Phi$  to be used in Eq. (10) and the propagation and SNR performance when code #4 in Table I is used. The net data rate vs. distance curve is shown in Fig. 11. The blue points (from the right to the left) correspond to the modulation formats reported in Table VI (from the top to the bottom). The performance of square PM-QAM modulation formats is also shown as green squares.

TABLE VI  
VALUES OF ENTROPY  $H(P)$  AND PARAMETER  $\Phi$  IN EQ. (10) FOR TDHF MODULATIONS. THE ACHIEVABLE NET DATA RATE OF PM SIGNALS, THE MAXIMUM NUMBER OF SPANS THAT CAN BE REACHED AND THE CORRESPONDING SNR ARE ALSO SHOWN, UNDER THE ASSUMPTION THAT THE CODE #4 IN TABLE I IS USED.

QAM formats	$\frac{N_1}{N_2}$	H(P) [bits/symb]	$\Phi$	Rate [Gbit/s]	$N_s$	SNR [dB]
4/16-QAM	5/1	2.33	0.845	241.6	44	9.0
4/16-QAM	3/1	2.5	0.806	259.2	37	9.7
4/16-QAM	2/1	2.67	0.77	276.8	32	10.3
4/16-QAM	1/1	3	0.725	311.0	25	11.4
4/16-QAM	1/2	3.33	0.701	345.3	21	12.3
4/16-QAM	1/3	3.5	0.699	362.9	19	12.7
4/16-QAM	1/5	3.67	0.686	380.5	17	13.0
16/64-QAM	5/1	4.33	0.661	448.9	11	14.9
16/64-QAM	3/1	4.5	0.656	466.6	10	15.5
16/64-QAM	2/1	4.67	0.644	484.2	9	16.1
16/64-QAM	1/1	5	0.633	518.4	7	17.0
16/64-QAM	1/2	5.33	0.628	552.6	6	17.8
16/64-QAM	1/3	5.5	0.622	570.2	5	18.2
64/256-QAM	3/1	6.5	0.615	673.9	3	20.9
64/256-QAM	1/1	7	0.61	725.8	2	22.3

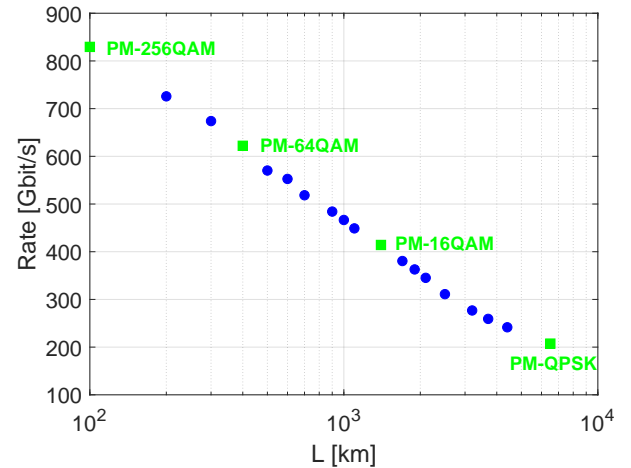


Fig. 11. Net data rate of polarization-multiplexed TDHFs vs. distance when the FEC code #4 in Table I is used. The blue circles (from the right to the left) corresponds to the modulation formats reported in Table VI (from the top to the bottom). The four green squares report the performance of square PM-QAM formats. The number of WDM channels is 60, corresponding to a total bandwidth of  $\sim 4.5$  GHz.

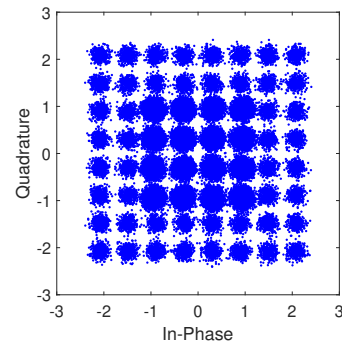


Fig. 12. Noisy scattering diagrams of the TDHF with  $H(P)=4.5$  bits/symb (see Table VI).

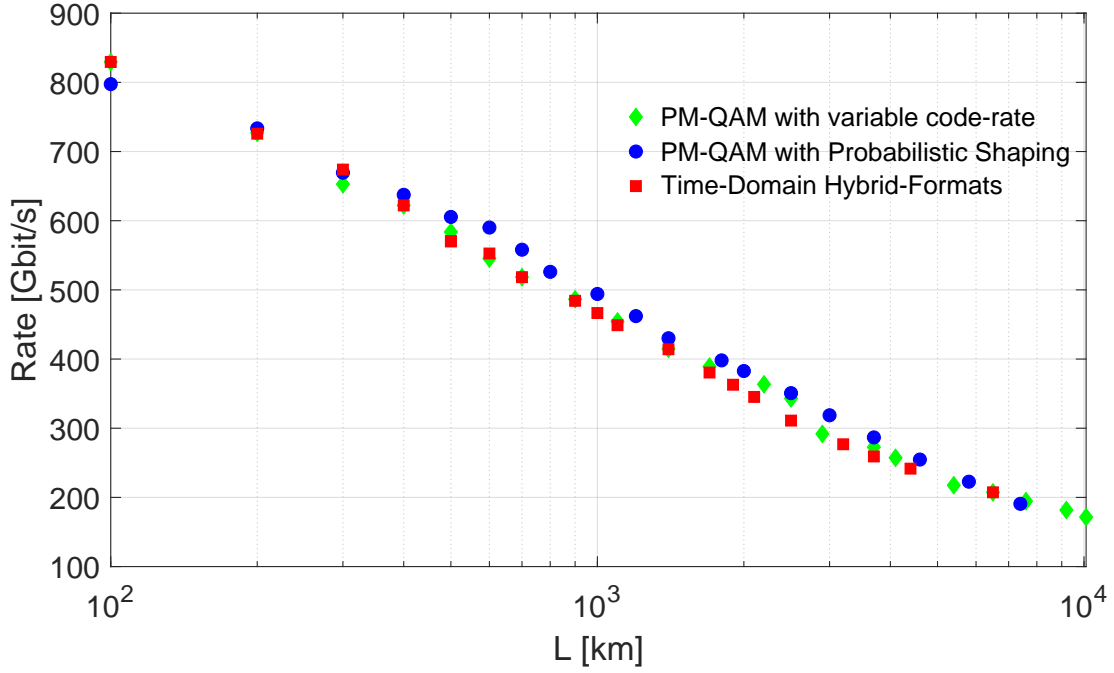


Fig. 13. Comparison of rate-reach trade-off for the three analyzed modulation schemes (derived from the data reported in Figs. 5, 9 and 11).

An example of TDHF constellation can be seen in Fig. 12, where the noisy scattering diagram of a hybrid format composed of a frame of three 16QAM symbols and one 64-QAM symbol is shown. The achieved entropy is equal to 4.5 bits/symb. Note that this plot highlights how TDHFs can be considered as an alternative way to perform probabilistic constellation shaping. However, the achieved distribution is far from the optimum Gaussian one, and thus there is no significant performance improvement with respect to uniformly distributed constellations, as also shown by the results in Fig. 11.

## V. MODULATION SCHEMES COMPARISON

Fig. 13 compares the rate versus reach results obtained using the three modulation schemes described in Section IV over a common multi-span propagation scenario whose parameters are reported in Table II. The application of PS on a QAM modulation format makes the constellation shape closer to a Gaussian distribution, which, in accordance with the Shannon's theorem, ideally allows to achieve the channel capacity in an AWGN channel. For this reason, as also experimentally demonstrated in several works [17]–[21], the performance of PS formats is slightly better than uniform QAM and TDHF, with higher gains in the region [500–2000] km, [400–600] Gbit/s.

The results of Fig. 13 show that a good granularity is achieved in all cases, at the expenses of an increase in implementation complexity. For instance, when using PM-QAM formats with variable code rate, the required hardware effort for implementation of several FEC encoders and decoders in order to support the various code rates is significant and may lead to an undesired increase of transceiver cost [27]. In addition, the use of very large FEC overheads allows the

system to operate at very low SNR values, leading to a high symbol error rate, which can be challenging for DSP subsystems that rely on the feedback from symbol decisions.

On the other hand, most of the current PS investigations make use of a constant composition distribution matcher [84], which is known to pose several implementation issues, such as the requirement of very long blocks of bits to achieve the best performance, thus increasing latency and complexity. Therefore, simplified PS implementations have recently become very active research topics [89], [90]. In addition, despite of the shaping gain in linear regime due to its quasi-Gaussian distribution, PS is more impacted by the accumulation of nonlinear interference [79], which results in an enhanced nonlinear phase noise (NLPN) distortion [80].

In general, the generation and detection of TDHF pose less challenges than for PS signals. In [28] it was demonstrated that the TDHFs can be generated and easily re-configured using DAC enabled transmitters with linear modulators and RF drivers. The DSP required to process the TDHF signal at the receiver is described in Section III in [26], where it is also shown that the computational complexity can be as low as that in conventional single format transceivers. However, even if the composition of hybrid formats is optimized, the SNR performance is still far from that of the optimum Gaussian constellation [29], [30], as it is also shown in Fig. 13. Moreover, it has been shown that, due to the power unbalance between formats that is required to have them operating in similar conditions, the time multiplexing of QAM formats leads to additional nonlinear penalties, which appear to increase with the time frame length [29].

Note that the performance of uniformly distributed formats could be improved by using geometrical shaping (GS), i.e. by designing non-square constellations with a Gaussian-like

distribution of points and equal transmission probability for all symbols [63], [85]–[87]. However, PS has some advantages over GS in terms of flexibility, e.g. the net data rate can be adjusted with arbitrary granularity and the same DSP unit can be used to equalize the signal at different spectral efficiencies. In addition, using PS a sensitivity gain in the order of 1 dB can be achieved with respect to standard QAM constellations [18], [20], whilst a more limited gain can typically be obtained with GS [88]. Moreover, being based on non-standard QAM formats, these options face the challenge of requiring dedicated and potentially more complex DSP algorithms for their generation and processing.

## VI. SUB-CARRIER MULTIPLEXING (SCM)

This technique consists in electrically decomposing a high symbol-rate signal into a given number of electrical subcarriers (SCs), each of which operating at a lower symbol-rate [34]. SCM is also known in the literature as *Nyquist-FDM* [91]–[93]. In Nyquist-FDM signals the cross-talk between adjacent subcarriers is avoided by using a tight spectral shaping on the electrical subcarriers. Depending on the optical system under test, several degrees of freedom can be optimized, such as the number of sub-carrier components, the inter-subcarrier spacing and the associated modulation format and pulse shaping.

The granularity of the SCs allows to control the symbol duration by keeping a constant overall bandwidth. This ability of optimizing the symbol duration allows to adapt the signal for non-linearity tolerance and can therefore be used to extend the reach of optical transport systems [34], [83]. Furthermore, Nyquist-FDM allows flexible adaption of the bandwidth [94], power and modulation format [33] of each individual subcarrier. This allows for a flexible design of the spectral efficiency and therefore a finer granularity in transmission reach. Moreover, with a proper choice of the modulation format to be assigned to each subcarrier in the Nyquist-FDM frame, the effects of selective filtering can be efficiently mitigated and the transmission rate maximized. In particular, for optical communications systems including a large number of reconfigurable optical add/drop multiplexers (ROADMs), it has been demonstrated that, due to the effect of optical filtering, the best way to perform subcarrier loading is by placing the lower-order QAM SCs in the frequency edges of the frame and the higher-order QAM tributaries in the central part of the frame [35], [97].

In [32], the use of frequency domain hybrid formats (FDHF), based on SCM, was proposed as a time-invariant alternative to TDHF able to achieve similar level of bit-rate granularity. A disadvantage of SCM schemes is their larger sensitivity to transmitter impairments, like the IQ time imbalance, which needs a more precise calibration or additional calibration algorithms [95], [96]. In order to improve the performance of either TDHF or FDHF, polarization interleaving can be applied to equalize the power distribution in time or in the channel spectrum, respectively, also having beneficial effects in non-linear propagation, as shown in [31].

In the following, an example of combination of SCM with the three techniques described in Section IV is reported,

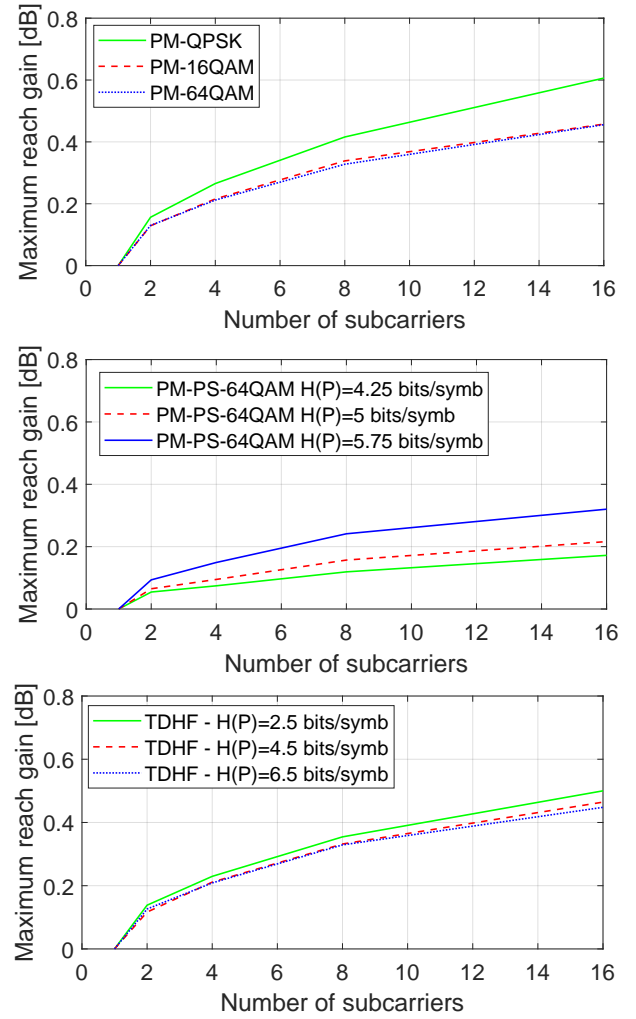


Fig. 14. Maximum reach gain (in dB) vs. the number of subcarriers for three modulation formats for each category (top: variable-rate QAM, middle: PS-QAM, bottom: TDHF). The number of WDM channels is 60, corresponding to a total bandwidth of  $\sim 4.5$  GHz.

showing that a performance gain is obtained thanks to the non-linearity reduction enabled by the SRO effect [38]. Fig. 14 shows the maximum reach gain (in dB) as a function of the number of subcarriers. The system parameters are those reported in Table II. The aggregate symbol rate is  $R_s=64$  Gbaud. The symbol rate of each SC is equal to  $R_s/N_{sc}$ , where  $N_{sc}$  is the number of subcarriers. The absolute maximum reach performance for the single-carrier systems can be found in Tables III, VI and V. The effects of symbol rate optimization (SRO) are evident in Fig. 14 for all the analyzed formats (three examples, with different entropy values, are shown for each modulation technique). Note that the SRO gain is higher for uniformly distributed formats (either standard QAM or TDHF) than for PS formats, as also demonstrated in [98]. This is due to the fact that the PS symbols approximate a Gaussian constellation, for which the effects of SRO are negligible. In practice, as also shown in [38], [99], the SRO gain is higher for modulation formats characterized by a higher value of the parameter  $\Phi$  in Eq. (11) (see Tables III, VI and V, where the values of  $\Phi$  are reported for all modulation formats considered in this paper). These results indicate that PS and

Gaussian-like constellations are not only more impacted by nonlinear phase noise, but also benefit less from the SRO gain. In addition, whilst in single-subcarrier systems part of the NLPN is efficiently compensated for by the feed-forward CPE algorithms that are used to mitigate laser phase noise, when increasing the number of sub-carriers the memory of NLPN in number of symbols becomes too short to be compensated for by standard CPE algorithms [100]. This further reduces the SRO gain for modulation formats affected by a strong NLPN, such as multi-level formats with Gaussian-like distribution. In conclusion, the combination of PS and SRO might not be as beneficial as the combination of standard QAM and SRO is.

## VII. CONCLUSION

A first step towards flexible networks that avoids the replacement of fibers and link components, like multiplexers, demultiplexers and ROADMs, consists in keeping fixed-grid dense WDM transmission on the installed equipment and introducing flexibility only through the replacement of transceivers. For this reason, the design of optical transceivers able to dynamically adapt the transmission rate to the channel conditions has been the goal of intense research activities in the past few years.

In this paper, three advanced modulation techniques that have been recently proposed to increase the flexibility of optical transceivers have been reviewed, i.e. QAM formats with variable code-rate, time-domain hybrid formats and probabilistic constellation shaping. Using a common reference multi-span propagation system scenario, the performance of all considered modulation schemes was assessed, in either a single-carrier or multi-subcarrier configuration.

All considered modulation schemes allow to achieve a good granularity in terms of combination of net data rate and transmission distance, at the expenses of an increase in the complexity of the DSP algorithms. One of the main challenges in the next years will be the development of efficient but simple Tx and Rx DSP algorithms for these class of advanced modulation schemes, which will enable a cost-efficient realization of flexible transceivers for next generation optical networks.

## ACKNOWLEDGMENT

The author would like to thank Andrea Carena, Vittorio Curri, Roberto Gaudino, Dario Pileri and Pierluigi Poggiolini from Politecnico di Torino, Antonello Nespola from Istituto Superiore Mario Boella, Chris Fludger and Fabrizio Forghieri from CISCO Systems, for the fruitful discussions.

## REFERENCES

- [1] X. Liu, S. Chandrasekhar, P. J. Winzer, "Digital Signal Processing Techniques Enabling Multi-Tb/s Superchannel Transmission: An overview of recent advances in DSP-enabled superchannels," *IEEE Signal Process. Mag.*, vol. 31, no. 2, pp. 16–24, Feb. 2014.
- [2] Md. S. Faruk, S. J. Savory, "Digital Signal Processing for Coherent Transceivers Employing Multilevel Formats," *J. Lightwave Technol.*, vol. 35, no. 5, pp. 1125–1141, Mar. 2015.
- [3] O. Gerstel, M. Jinno, A. Lord, S.J. Ben Yoo, "Elastic optical networking: A new dawn for the optical layer?," *IEEE Signal Process. Mag.*, vol. 50, no. 2, pp. s12–s20, Feb. 2012.
- [4] M. Jinno, H. Takara, B. Kozicki, Y. Tsukishima, Y. Sone, S. Matsuoka, "Spectrum-efficient and scalable elastic optical path network: Architecture, benefits, and enabling technologies," *IEEE Signal Process. Mag.*, vol. 47, no. 11, pp. 66–72, Nov. 2009.
- [5] K. Roberts, C. Laperle, "Flexible transceivers," in *Proc. Europ. Conf. Opt. Commun. (ECOC)*, Amsterdam (The Netherlands), Sep. 2012, paper We.3.A.3.
- [6] B. T. Teipen, M. Eiselt, K. Grobe, J.-P. Elbers, "Adaptive Data Rates for Flexible Transceivers in Optical Networks," *Journal of Networks*, vol. 7, no. 5, pp. 776–782, May 2012.
- [7] K. Roberts *et al.*, "High capacity transport - 100G and beyond," *J. Lightwave Technol.*, vol. 33, no. 3, pp. 563–578, Feb. 2015.
- [8] D. A. Morero *et al.*, "Design tradeoffs and challenges in practical coherent optical transceiver implementations," *J. Lightwave Technol.*, vol. 34, no. 1, pp. 121–136, Jan. 2016.
- [9] K. Roberts, Q. Zhuge, I. Monga, S. Gareau, C. Laperle, "Beyond 100 Gb/s: Capacity, Flexibility, and Network Optimization," *J. Opt. Commun. Netw.*, vol. 9, no. 4, pp. C12–C24, Apr. 2017.
- [10] X. Zhou *et al.*, "Flexible Transceivers: Extracting More Capacity from Elastic Meshed Optical Networks," in *Proc. Asia Comm. and Photon. Conf. (APC)*, Guangzhou (China), Nov. 2017, paper S4C.1.
- [11] G. Bosco, "Flexible Transceivers and the Rate/Reach Trade-off," in *Proc. Opt. Fiber Commun. Conf. (OFC)*, San Diego (USA), Mar. 2018, Paper M1G.1.
- [12] G.-H. Gho, J. M. Kahn, "Rate-adaptive modulation and coding for optical ber transmission systems," *J. Lightw. Technol.*, vol. 30, no. 12, pp. 1818–1828, Jun. 2012.
- [13] D. A. A. Mello *et al.*, "Optical networking with variable-code-rate transceivers," *J. Lightwave Technol.*, vol. 32, no. 2, pp. 257–266, Jan. 2014.
- [14] A. Alvarado, E. Agrell, D. Lavery, R. Maher, P. Bayvel, "Replacing the Soft-Decision FEC Limit Paradigm in the Design of Optical Communication Systems," *J. Lightw. Technol.*, vol. 34, no. 2, pp. 707–721, Jan. 2016.
- [15] D. J. Ives, A. Alvarado, S. J. Savory, "Throughput Gains From Adaptive Transceivers in Nonlinear Elastic Optical Networks," *J. Lightw. Technol.*, vol. 35, no. 6, pp. 1280–1289, Mar. 2017.
- [16] A. L. N. Souza *et al.*, "Parameter selection in optical networks with variable-code-rate superchannels," *J. Optical Comm. Netw.*, vol. 8, no. 7, pp. A152–A161, Jul. 2016.
- [17] M. P. Yankov, D. Zibar, K. J. Larsen, L. P. B. Christensen, S. Forchhammer, "Constellation shaping for ber-optic channels with QAM and high spectral efficiency," *IEEE Photon. Technol. Lett.*, vol. 26, no. 23, pp. 2407–2410, Dec. 2014.
- [18] F. Buchali, F. Steiner, G. Boecherer, L. Schmalen, P. Schulte, W. Idler, "Rate adaptation and reach increase by probabilistically shaped 64-QAM: An experimental demonstration," *J. of Lightw. Technol.*, vol. 34, no. 7, pp. 1599–1609, April 2016.
- [19] F. R. Kschischang *et al.*, "Probabilistic 16-QAM Shaping in WDM Systems," *J. Lightw. Technol.*, vol. 34, no. 18, pp. 4285–4292, Sep. 2016.
- [20] D. Pileri, L. Bertignono, A. Nespola, F. Forghieri, G. Bosco, "Comparison of Probabilistically Shaped 64QAM with Lower-Cardinality Uniform Constellations in Long-Haul Optical Systems," *J. Lightwave Technol.*, vol. 37, no. 2, pp. 501–509, Jan. 2018.
- [21] S. Chandrasekhar *et al.*, "High-spectral-efficiency transmission of PDM 256-QAM with Parallel Probabilistic Shaping at Record Rate-Reach Trade-offs," in *Proc. Europ. Conf. Opt. Commun. (ECOC)*, Dusseldorf (Germany), Sep. 2016, paper Th.3.C.1.
- [22] D. Pileri, G. Bosco, C. Fludger, "Impact of finite-resolution DAC and ADC on probabilistically-shaped QAM constellations," in *Proc. IEEE Photonics Conference (IPC)*, Orlando (USA), Oct. 2017, pp. 433–434.
- [23] D. Pileri, F. Forghieri, G. Bosco, "Maximization of the achievable mutual information using probabilistically shaped squared QAM constellations," in *Proc. Opt. Fiber Commun. Conf. (OFC)*, Los Angeles (USA), Mar. 2017, Paper W2A.57.
- [24] W.-R. Peng, I. Morita, H. Tanaka, "Hybrid QAM transmission techniques for single-carrier ultra-dense WDM systems," in *Proc. Optoelectron. Commun. Conf.*, 2011, pp. 824–825.
- [25] X. Zhou *et al.*, "4000 km transmission of 50 GHz spaced, 10 494.85-Gb/s hybrid 3264 QAM using cascaded equalization and training-assisted phase recovery," in *Proc. Opt. Fiber Commun. Conf. (OFC)*, Los Angeles (USA), Mar. 2012, Paper PDP5C.6.
- [26] Q. Zhuge *et al.*, "Spectral efficiency-adaptive optical transmission using time domain hybrid QAM for agile optical networks," *J. Lightw. Technol.*, vol. 31, n. 15, pp. 2621–2628, Aug. 2013.



- [27] X. Zhou, L. E. Nelson, P. Magill, "Rate-adaptable optics for next generation long-haul transport networks," *IEEE Comm. Mag.*, vol. 51, no. 3, pp. 41–49, Mar. 2013.
- [28] Q. Zhuge, X. Xu, M. Morsy-Osman, M. Chagnon, M. Qiu, D. V. Plant, "Time domain hybrid QAM based rate-adaptive optical transmissions using high speed DACs," in *Proc. Opt. Fiber Commun. Conf. (OFC)*, Anaheim (USA), Mar. 2017, pp. 1–3.
- [29] V. Curri *et al.*, "Time-Division Hybrid Modulation Formats: Tx Operation Strategies and Countermeasures to Nonlinear Propagation," in *Proc. Opt. Fiber Commun. Conf. (OFC)*, San Francisco (USA), Mar. 2014, paper Tu3A.2.
- [30] F. Buchali, L. Schmalen, K. Schuh, W. Idler, "Optimization of time-division hybrid-modulation and its application to rate adaptive 200 Gb transmission," in *Proc. Europ. Conf. Opt. Commun. (ECOC)*, Cannes (France), Sep. 2014, paper Tu.4.3.1.
- [31] F. P. Guiomar *et al.*, "Hybrid modulation formats enabling elastic fixed-grid optical networks," *J. Opt. Commun. Netw.*, vol. 8, n. 7, pp. A92–A100, Jul. 2016.
- [32] F. P. Guiomar, A. Carena, "Achieving Fine Bit-Rate Granularity with Hybrid Subcarrier Modulation," in *Proc. Signal Processing in Photonic Communications (SPPCom)*, paper Sp.W3F.2 (2016).
- [33] D. Krause, A. Awadalla, A. Karar, H. Sun, K.-T. Wu, "Design Considerations for a Digital Subcarrier Coherent Optical Modem," in *Proc. Opt. Fiber Commun. Conf.*, Los Angeles (USA), 2017, Paper Th1D.1.
- [34] M. Qiu *et al.*, "Digital subcarrier multiplexing for fiber nonlinearity mitigation in coherent optical communication systems," *Opt. Express*, vol. 22, n. 15, pp. 18770–18777, 2014.
- [35] T. Rahman *et al.*, "Digital subcarrier multiplexed hybrid QAM for data-rate flexibility and ROADM filtering tolerance," in *Proc. Opt. Fiber Commun. Conf. (OFC)*, Anaheim (USA), 2016, Paper Tu3K.5.
- [36] X. Meng *et al.*, "Filtering Tolerant Digital Subcarrier Multiplexing System with Flexible Bit and Power Loading," in *Proc. Opt. Fiber Commun. Conf. (OFC)*, Los Angeles (USA), 2017, Paper W4A.7.
- [37] F. P. Guiomar *et al.*, "Comparing Different Options for Flexible Networking: Probabilistic Shaping vs. Hybrid Subcarrier Modulation," in *Proc. Europ. Conf. Opt. Commun. (ECOC)*, Gothenburg (Sweden), Sep. 2017, paper Th1E.3.
- [38] P. Poggiolini *et al.*, "Analytical and experimental results on system maximum reach increase through symbol rate optimization," *J. Lightw. Technol.*, vol. 34, n. 8, pp. 1872–1885, Apr. 2016.
- [39] J. M. Kahn, K. -P. Ho, "Spectral efficiency limits and modulation/detection techniques for DWDM systems," *IEEE J. Sel. Topics Quantum Electron.*, vol. 10, no. 2, pp. 259–272, Mar./Apr. 2004.
- [40] P. Winzer, "High-Spectral-Efficiency Optical Modulation Formats," *J. Lightwave Technol.*, vol. 30, no. 24, pp. 3824–3835, Dec. 2012.
- [41] G. Bosco, V. Curri, A. Carena, P. Poggiolini, F. Forghieri, "On the Performance of Nyquist-WDM Terabit Superchannels Based on PM-BPSK, PM-QPSK, PM-8QAM or PM-16QAM Subcarriers," *J. Lightw. Technol.*, vol. 29, no. 1, Jan. 2011, pp. 53–61.
- [42] G. Bosco, "Spectral Shaping in Ultra-Dense WDM Systems: Optical vs. Electrical Approaches," in *Proc. Opt. Fiber Commun. Conf. (OFC)*, Los Angeles (USA), 2012, Paper OM3H.1.
- [43] C. Laperle, M. O. Sullivan, "Advances in high-speed DACs, ADCs, and DSP for optical coherent transceivers," *J. Lightwave Technol.*, vol. 32, no. 4, pp. 629–643, Feb. 2014.
- [44] K. Kikuchi, "Fundamentals of Coherent Optical Fiber Communications," *J. Lightw. Technol.*, vol. 34, no. 1, Jan. 2016, pp. 157–179.
- [45] S. J. Savory, "Digital coherent optical receivers: Algorithms and subsystems," *IEEE J. Sel. Topics Quantum Electron.*, vol. 16, no. 5, pp. 1164–1179, May 2010.
- [46] T. Pfau, S. Hoffmann, R. Noe, "Hardware-Efficient Coherent Digital Receiver Concept With Feedforward Carrier Recovery for M-QAM Constellations," *J. Lightwave Technol.*, vol. 27, no. 8, pp. 989–999, Apr. 2009.
- [47] M. Seimetz, "Laser Linewidth Limitations for Optical Systems with High-Order Modulation Employing Feed Forward Digital Carrier Phase Estimation," in *Proc. Opt. Fiber Commun. Conf. (OFC)*, San Diego (USA), Mar. 2008, Paper Paper OTuM2.
- [48] R. Schmogrow, S. Ben-Ezra, P. C. Schindler, B. Nebendahl, C. Koos, W. Freude, J. Leuthold, "Pulse-Shaping With Digital, Electrical, and Optical Filters: A Comparison," *J. Lightw. Technol.*, vol. 31, no. 15, Aug. 2013, pp. 2570–2577.
- [49] M. Mazurczyk, "Spectral Shaping in Long Haul Optical Coherent Systems With High Spectral Efficiency," *J. Lightw. Technol.*, vol. 32, no. 16, Aug. 2014, pp. 2915–2924.
- [50] D. Rafique, T. Rahman, A. Napoli, B. Spinnler, "Digital Pre-Emphasis in Optical Communication Systems: On the Nonlinear Performance," *J. Lightwave Technol.*, vol. 33, no. 1, pp. 140–150, Jan. 2015.
- [51] G. Khanna, S. Calabrò, B. Spinnler, E. De Man, N. Hanik, "Joint adaptive pre-compensation of transmitter I/Q skew and frequency response for high order modulation formats and high Baud rates," in *Proc. Opt. Fiber Commun. Conf. (OFC)*, Los Angeles (USA), Mar. 2015, Paper M2G.4.
- [52] T. Nguyen, *et al.*, "Blind Transmitter IQ Imbalance Compensation in M-QAM Optical Coherent Systems," *J. Opt. Commun. Netw.*, vol. 9, no. 9, pp. D42–D50, Sep. 2017.
- [53] P. W. Berenguer *et al.*, "Nonlinear Digital Pre-distortion of Transmitter Components," *J. Lightw. Technol.*, vol. 34, no. 8, pp. 1739–1745, Apr. 2016.
- [54] G. Khanna *et al.*, "A Robust Adaptive Pre-Distortion Method for Optical Communication Transmitters," *IEEE Photon. Technol. Lett.*, vol. 28, no. 7, pp. 752–755, Apr. 2016.
- [55] S. J. Savory, "Optimum electronic dispersion compensation strategies for nonlinear transmission," *Electronics Lett.*, vol. 42, no. 7, pp. 407–408, Jul. 2006.
- [56] A. Ghazisaeidi, J. Renaudier, M. Salsi, P. Tran, G. Charlet, S. Bigo, "System benefits of digital dispersion pre-compensation for non-dispersion-managed PDM-WDM transmission," in *Proc. Europ. Conf. Opt. Commun. (ECOC)*, London (UK), Sep. 2013, paper We.4.D.4.
- [57] K. Roberts, C. Li, L. Strawczynski, M. O'Sullivan, I. Hardcastle, "Electronic precompensation of optical nonlinearity," *IEEE Photon. Technol. Lett.*, vol. 18, no. 2, pp. 403–405, Jan. 2006.
- [58] E. Temprana *et al.*, "Two-fold transmission reach enhancement enabled by transmitter-side digital backpropagation and optical frequency comb-derived information carriers," *Opt. Exp.*, vol. 23, no. 16, pp. 20774–20783, 2015.
- [59] D. Lavery, D. Ives, G. Liga, A. Alvarado, S. Savory, P. Bayvel, "The benefit of split nonlinearity compensation for single channel optical fiber communications," *IEEE Photon. Technol. Lett.*, vol. 28, no. 17, pp. 1803–1806, Sep. 2016.
- [60] E. Ip, J. M. Kahn, "Digital equalization of chromatic dispersion and polarization mode dispersion," *J. Lightw. Technol.*, vol. 25, no. 8, pp. 2033–2043, Aug. 2007.
- [61] S. J. Savory, "Digital filters for coherent optical receivers," *Opt. Express*, vol. 16, no. 2, pp. 804–817, 2008.
- [62] M. Kuschnerov *et al.*, "DSP for coherent single-carrier receivers," *J. Lightw. Technol.*, vol. 27, no. 16, pp. 3614–3622, Aug. 2009.
- [63] J. K. Fischer *et al.*, "Bandwidth-variable transceivers based on four-dimensional modulation formats," *J. Lightw. Technol.*, vol. 32, n. 16, pp. 2886–2895, Aug. 2014.
- [64] I. Fatadin, D. Ives, S. J. Savory, "Blind Equalization and Carrier Phase Recovery in a 16-QAM Optical Coherent System," *J. Lightw. Technol.*, vol. 27, n. 15, pp. 3042–3049, Aug. 2009.
- [65] D. S. Millar, S. J. Savory, "Blind adaptive equalization of polarization switched QPSK modulation," *Opt. Exp.*, vol. 19, no. 9, pp. 8533–8538, 2011.
- [66] X. Zhou, "An improved feed-forward carrier recovery algorithm for coherent receivers with M-QAM modulation format," *IEEE Photon. Technol. Lett.*, vol. 22, no. 14, pp. 1051–1053, Jul. 2010.
- [67] Q. Zhuge *et al.*, "Terabit bandwidth-adaptive transmission using low-complexity format-transparent digital signal processing," *Opt. Express*, vol. 22, no. 3, pp. 2278–2288, 2014.
- [68] A. P. T. Lau *et al.*, "Advanced DSP techniques enabling high spectral efficiency and flexible transmissions: Toward elastic optical networks," *IEEE Signal Process. Mag.*, vol. 31, no. 2, pp. 82–92, Feb. 2014.
- [69] R. Elschnner, F. Frey, C. Schmidt-Langhorst, J. K. Fischer, C. Schubert, "Data-Aided DSP for Flexible Transceivers," in *Proc. Advanced Photonics for Commun. 2014*, San Diego (USA), Jul. 2014, paper SW1C.1.
- [70] M. Morsy-Osman, Q. Zhuge, L. R. Chen, D. V. Plant, "Feedforward carrier recovery via pilot-aided transmission for single-carrier systems with arbitrary M-QAM constellations," *Opt. Exp.*, vol. 19, no. 24, pp. 24331–24343, Nov. 2011.
- [71] T. Kobayashi, A. Sano, A. Matsuura, Y. Miyamoto, K. Ishihara, "Nonlinear tolerant spectrally-efficient transmission using PDM 64-QAM single carrier FDM with digital pilot-tone," *J. Lightw. Technol.*, vol. 30, no. 24, pp. 3805–3815, Dec. 2012.
- [72] R. Schmogrow, M. Meyer, P. C. Schindler, A. Josten, S. Ben-Ezra, C. Koos, W. Freude, J. Leuthold, "252 Gbit/s Real-Time Nyquist Pulse Generation by Reducing the Oversampling Factor to 1.33," in *Proc. Opt. Fiber Commun. Conf. (OFC)*, Anaheim (USA), Mar. 2013, Paper Paper OTu2I.1.

- [73] A. Nespola *et al.*, “1306-km 20x124.8-Gb/s PM-64QAM Transmission over PSCF with Net SEDP 11,300 (bkm)/s/Hz using 1.15 samp/symb DAC,” *Opt. Express*, vol. 22, no. 1, pp. 1796–1805, 2014.
- [74] R. A. Griffin, A. C. Carter, “Optical differential quadrature phase-shift key (oDQPSK) for high capacity optical transmission,” in *Proc. Opt. Fiber Commun. Conf. (OFC)*, Anaheim (USA), Mar. 2002, Paper Paper WX6.
- [75] J. Cho, L. Schmalen, P. Winzer, “Normalized Generalized Mutual Information as a Forward Error Correction Threshold for Probabilistically Shaped QAM,” in *Proc. Europ. Conf. of Opt. Commun. (ECOC)*, Gothenburg (Sweden), 2017, Paper M.2.D.2.
- [76] A. Alvarado, T. Fehenberger, Bin Chen, F.M.J. Willems, “Achievable Information Rates for Fiber Optics: Applications and Computations,” *J. Lightw. Technol.*, vol. 36, no. 2, pp. 424–439, Jan. 2018.
- [77] L.M. Zhang, F.R. Kschischang, “Staircase codes with 6% to 33% overhead,” *J. Lightw. Technol.*, vol. 32, no. 10, pp. 1999–2002, May 2014.
- [78] G. Boecherer, F. Steiner, P. Schulte, “Bandwidth efficient and rate-matched low-density parity-check coded modulation,” *IEEE Trans. Commun.*, vol. 63, no. 12, pp. 4651–4665, Dec. 2015.
- [79] A.Carena, G. Bosco, V. Curri, Y. Jiang, P. Poggiolini, F. Forghieri, “EGN model of non-linear fiber propagation,” *Opt. Express*, vol. 22, no. 13, pp. 16335–16362, 2014.
- [80] R. Dar, M. Feder, A. Mecozzi, M. Shtaf, “Inter-Channel Nonlinear Interference Noise in WDM Systems: Modeling and Mitigation,” *J. Lightw. Technol.*, vol. 33, no. 5, pp. 1044–1053, Mar. 2015.
- [81] P. Poggiolini, Y. Jiang “Recent Advances in the Modeling of the Impact of Nonlinear Fiber Propagation Effects on Uncompensated Coherent Transmission Systems,” *J. Lightw. Technol.*, vol. 35, no. 3, pp. 458–480, Feb. 2017.
- [82] P. Poggiolini, G. Bosco, A. Carena, V. Curri, Y. Jiang and F. Forghieri, “A Simple and Effective Closed-Form GN Model Correction Formula Accounting for Signal Non-Gaussian Distribution,” *J. Lightw. Technol.*, vol. 33, no. 2, pp. 459–473, Jan. 2015.
- [83] P. Poggiolini, G. Bosco, A. Carena, V. Curri, Y. Jiang, F. Forghieri, “The GN-Model of Fiber Non-Linear Propagation and its Applications,” *J. Lightw. Technol.*, vol. 32, no. 4, pp. 694–721, Feb. 2014.
- [84] P. Schulte, G. Boecherer, “Constant Composition Distribution Matching,” *IEEE Trans. Inf. Theory*, vol. 62, no. 1, pp. 430–434, Jan. 2016.
- [85] E. Agrell, M. Karlsson, “Power-efficient modulation formats in coherent transmission systems,” *J. Lightw. Technol.*, vol. 27, no. 22, pp. 5115–5126, Nov. 2009.
- [86] T. Liu, I. B. Djordjevic, “On the optimum signal constellation design for high-speed optical transport networks,” *Opt. Express*, vol. 20, no. 18, pp. 20396–20406, Aug. 2012.
- [87] D. S. Millar *et al.*, “High-dimensional modulation for coherent optical communications systems,” *Opt. Express*, vol. 22, no. 7, pp. 798–8812, Apr. 2014.
- [88] F. Steiner, G. Boecherer, “Comparison of Geometric and Probabilistic Shaping with Application to ATSC 3.0,” in *Proc. International ITG Conf. on Systems, Commun. and Coding (SCC)*, Hamburg (Germany), 2017, pp. 1–6.
- [89] J. Cho, S. Chandrasekhar, R. Dar, P. J. Winzer, “Low-complexity shaping for enhanced nonlinearity tolerance,” in *Proc. Europ. Conf. of Opt. Commun. (ECOC)*, Dusseldorf (Germany), Sep. 2016, pp. 467–469.
- [90] M. Pikus, W. Xu, “Bit-level probabilistically shaped coded modulation,” *IEEE Commun. Lett.*, vol. 21, no. 9, pp. 1929–1932, Sep. 2017.
- [91] R. Schmogrow, S. Wolf, B. Baeuerle, D. Hillerkuss, B. Nebendahl, C. Koos, W. Freude, J. Leuthold, “Nyquist Frequency Division Multiplexing for Optical Communications,” *Proc. Conf. on Lasers and Electro-Optics (LEOS)*, San Jose (USA), 2012, paper CThI.2.
- [92] L. Dou, X. Su, Y. Fan, H. Chen, Y. Zhao, Z. Tao, T. Tanimura, T. Hoshida, J. Rasmussen, “420Gbit/s DP-64QAM Nyquist-FDM Single-Carrier System,” in *Proc. Opt. Fiber Commun. Conf. (OFC)*, Anaheim (USA), Mar. 2016, Paper Tu3A.5.
- [93] B. Baeuerle, A. Josten, M. Eppenberger, D. Hillerkuss, J. Leuthold, “FPGA-based Realtime Receivers for Nyquist-FDM,” *Proc. Advanced Photonics 2017*, New Orleans (USA), 2017, paper SpM3F.3.
- [94] P. C. Schindler, R. Schmogrow, S. Wolf, B. Baeuerle, B. Nebendahl, C. Koos, W. Freude, J. Leuthold, “Full flex-grid asynchronous multiplexing demonstrated with Nyquist pulse-shaping,” *Opt. Express*, vol. 22, no. 9, pp. 10923–10937, 2014.
- [95] G. Bosco *et al.*, “Impact of the transmitter IQ-skew in multi-subcarrier coherent optical systems,” in *Proc. Opt. Fiber Commun. Conf. (OFC)*, Anaheim (USA), Mar. 2016, Paper W4A.5.
- [96] B. Baeuerle, A. Josten, R. Bonjour, D. Hillerkuss, J. Leuthold, “Effect of Transmitter Impairments on Nyquist-FDM Signals with Increasing Sub-band Granularity,” in *Proc. Advanced Photonics 2016*, Vancouver (Canada), Jul. 2016, paper SpW3F.4.
- [97] F. P. Guiomar, L. Bertignono, A. Nespola, A. Carena, “Frequency-Domain Hybrid Modulation Formats for High Bit-Rate Flexibility and Nonlinear Robustness,” *J. Lightw. Technol.*, vol. 36, no. 20, pp. 4856–4870, Oct. 2018.
- [98] P. Poggiolini, G. Bosco, A. Carena, D. Pileri, A. Nespola, M. Ranjbar Zefreh, M. Bertino, F. Forghieri, “Non-Linearity Modeling for Gaussian-Constellation Systems at Ultra-High Symbol Rates,” in *Proc. Europ. Conf. of Opt. Commun. (ECOC)*, Rome (Italy), Sep. 2018, Paper Tu4G.3.
- [99] R. Dar, P. J. Winzer, “Nonlinear Interference Mitigation: Methods and Potential Gain,” *J. Lightw. Technol.*, vol. 35, no. 4, pp. 903–930, Feb. 2017.
- [100] D. Pileri, F. Forghieri, G. Bosco, “Residual Non-Linear Phase Noise in Probabilistically Shaped 64-QAM Optical Links,” in *Proc. Opt. Fiber Commun. Conf. (OFC)*, San Diego (USA), Mar. 2018, Paper M3C.6.

**Gabriella Bosco** (S’00–M’02–SM’13–F’19) received the Ph.D. degree in electronic and communication engineering from Politecnico di Torino, Italy, in 2002. In 2000, she was a Visiting Researcher with the University of California, Santa Barbara, CA, USA. From 1998 to 2011, she held a Postdoctoral position in the OptCom Group at Politecnico di Torino, where she worked as an Assistant Professor from 2011 to 2014. She currently is an Associate Professor at the Department of Electronics and Telecommunications and an elected member of the Academic Senate of Politecnico di Torino.

Her main research interests include the performance analysis and design of optical transmission systems and the application of digital signal processing techniques in optical links. She has coauthored several book chapters and more than 200 peer-reviewed papers in leading journals and conferences. In 2014 and 2015 she was one of the winners of the IEEE/OSA Journal of Lightwave Technology “Best Paper Award”.

Since 2011, she has served on the program committee of several international conferences (among which OFC, CLEO and IPC). She is currently serving as Editor-in-Chief of the IEEE/OSA Journal of Lightwave Technology, having previously served as Associate Editor from 2014 to 2017 and as Deputy Editor in 2018. She was Program Co-Chair of the Optical Fiber Communication conference (OFC) in 2017 and she is currently General Co-Chair for OFC 2019. Recently, she was elevated to Fellow of the OSA and the IEEE for contributions to modeling and design of coherent optical communication systems.